



1 **African Smoke Particles Act as Cloud Condensation Nuclei in the Wintertime Tropical**
2 **North Atlantic Boundary Layer over Barbados**

3 Haley M. Royer¹, Mira L. Pöhlker^{2,3,4*}, Ovid Krüger², Edmund Blades^{5,6}, Peter Sealy⁵, Nurun
4 Nahar Lata⁷, Zezhen Cheng⁷, Swarup China⁷, Andrew P. Ault⁸, Patricia K. Quinn⁹, Paquita
5 Zuidema¹, Christopher Pöhlker², Ulrich Pöschl², and Cassandra J. Gaston^{1*}

6 ¹Department of Atmospheric Sciences, Rosenstiel School of Marine and Atmospheric Science,
7 University of Miami, Miami, FL

8 ²Department of Multiphase Chemistry, Max Planck Institute for Chemistry, Mainz, Germany

9 ³Leipzig Institute for Meteorology, Leipzig University, Leipzig, Germany

10 ⁴Experimental Aerosol and Cloud Microphysics Department, Leibniz Institute for Tropospheric
11 Research, Leipzig, Germany

12 ⁵Barbados Atmospheric Chemistry Observatory, Ragged Point, Barbados

13 ⁶Queen Elizabeth Hospital Barbados, Bridgetown, Barbados

14 ⁷Environmental Molecular Sciences Laboratory, Pacific Northwest National Laboratory,
15 Richland, WA

16 ⁸Department of Chemistry, University of Michigan, Ann Arbor, MI

17 ⁹Pacific Marine Environmental Laboratory, National Oceanic and Atmospheric Administration,
18 Seattle, WA

19

20 *Corresponding Authors:



- 21 Mira L. Pöhlker: Email: pohlker@tropos.de, Phone: +49 6131 305 7020
- 22 Cassandra J. Gaston: Email: cgaston@rsmas.miami.edu, Phone: (305)-421-4979

23

24



25 **Abstract**

26 The number concentration and properties of aerosol particles serving as cloud condensation
27 nuclei (CCN) are important for understanding cloud formation, particularly in the tropical
28 Atlantic marine boundary layer (MBL) where marine cumulus clouds reflect incoming solar
29 radiation and obscure the low-albedo ocean surface. Studies linking aerosol source, composition,
30 and water uptake properties in this region have been conducted primarily during summertime
31 dust transport, despite the region receiving a variety of aerosol particle types throughout the year.
32 In this study, we compare size-resolved aerosol chemical composition data to the hygroscopicity
33 parameter κ derived from size-resolved CCN measurements made during the EUREC⁴A and
34 ATOMIC campaigns from January to February 2020. We observed unexpected periods of
35 wintertime long-range transport of African smoke and dust to Barbados. During these periods,
36 the accumulation mode aerosol particle and CCN number concentrations as well as the
37 proportions of dust and smoke particles increased while the average κ slightly decreased ($\kappa =$
38 0.45 ± 0.1) from marine background conditions ($\kappa = 0.52 \pm 0.08$) when the particles were mostly
39 composed of marine organics and sulfate. Size-resolved chemical analysis shows that smoke
40 particles were the major contributor to the accumulation mode aerosol during long-range
41 transport events, indicating that smoke is mainly responsible for the observed increase in CCN
42 number concentrations. Earlier studies conducted at Barbados have mostly focused on the role of
43 dust on CCN, but our results show that aerosol hygroscopicity and CCN number concentrations
44 during wintertime long-range transport events over the tropical North Atlantic are affected by
45 African smoke more than dust. Our findings highlight the importance of African smoke for
46 atmospheric processes and cloud formation over the Caribbean.

47



48 **Introduction**

49 Aerosol particle number, size, hygroscopicity, and chemical mixing state determine cloud
50 droplet formation and, thus, fundamentally affect the radiative properties and lifetime of clouds
51 (Albrecht, 1989; McFiggans et al., 2006; Quinn et al., 2008; Twomey, 1977; Zuidema et al.,
52 2008). Quantifying the effect of aerosols on cloud radiative forcing, however, is still the single
53 largest source of uncertainty in predicting temperature increases associated with climate change
54 (Forster et al., 2021). This uncertainty is especially important to resolve in marine regions where
55 aerosol-cloud interactions are understudied, even though the majority of Earth's surface is
56 covered by oceans (Carslaw et al., 2013). The existing literature that explores marine aerosol-
57 cloud interactions does so primarily in the mid to high latitudes of the North Atlantic with few
58 studies focusing in tropical latitudes where shallow cumulus clouds form (Allan et al., 2008;
59 Behrenfeld et al., 2019; Klingebiel et al., 2019; Rauber et al., 2007; Sorooshian et al., 2020).
60 Shallow cumulus clouds are important for Earth's climate as they are one of the most
61 geographically pervasive cloud types and can influence Earth's radiative budget by reflecting
62 incoming radiation over the low-albedo ocean surface.

63 Aerosol research conducted in the tropical Atlantic has focused mostly on the long-range
64 transport of mineral dust from North Africa in the summertime. Long-range African dust
65 transport occurs when emitted desert dust is lofted above the marine boundary layer (MBL) into
66 the Saharan Air Layer (SAL) and is propagated westward (Carlson & Prospero, 1972). As dust is
67 transported westward, it can mix into the underlying moist MBL and deposit into the Atlantic
68 Ocean and Caribbean Sea as well as Western Atlantic land masses such as South America, the
69 Caribbean islands, and North America (Barkley et al., 2019; Carlson & Prospero, 1972; Prospero et
70 al., 1981, 2020). Some studies have attempted to understand the effects of long-range transported



71 dust on cloud droplet formation and water uptake with varying results depending on the degree
72 of aging that dust experiences during transport (Allan et al., 2008; Denjean et al., 2015;
73 Rosenfeld et al., 2001). Ultimately, though, these studies provide conflicting results on whether
74 dust particles are hygroscopic and numerous enough to impact CCN concentrations and, thus, do
75 not thoroughly explain aerosol-cloud interactions in the tropical Atlantic. Due to the annual
76 oscillation of the intertropical convergence zone (ITCZ), dust transport also exhibits a
77 seasonality in terms of its geographic extent (Adams et al., 2012; Chin et al., 2014; Prospero &
78 Lamb., 2003; Prospero, 1968; Prospero & Mayol-Bracero, 2013; Yu et al., 2019; Zuidema et al., 2019).
79 However, marine shallow cumulus clouds form year-round in the tropical Atlantic regardless of
80 dust transport, suggesting that other marine or other long-range transported sources are important
81 for aerosol-cloud interactions in this region (McCoy et al., 2022).

82 Few studies have attempted to fully understand which aerosols are the most prominent
83 CCN both during dust seasons and non-dust seasons in the tropical North Atlantic MBL. One
84 particle type that may be important for CCN activation in the tropical north Atlantic yet has been
85 understudied at dust receptor sites such as Barbados is African smoke (Wex et al., 2016). In
86 contrast to dust, previous research has shown that smoke particles are an important source of
87 CCN (Edwards et al., 2021; Latham et al., 2013; Pierce et al., 2007; Spracklen et al., 2011) with
88 more recent research showing that some smoke particles can activate at supersaturations as low
89 as 0.05%.

90 There are a number of reasons that explain why smoke particles can be effective CCN.
91 Smoke particles are often complex mixtures of both organic and inorganic components that
92 change compositionally and morphologically during their residence time in the atmosphere (Reid
93 et al., 2005). Smoke properties may also vary between fires depending on fuel type and moisture,



94 combustion phase, wind conditions, etc. (Andreae, 2019; Miles et al., 1995; Reid et al., 2005). In
95 general, smoke particles are often found in the accumulation mode of the aerosol size
96 distribution and primarily contain particulate organic matter, black carbon, and inorganic
97 components including potassium chloride salts (Reid et al., 2005). Upon emission, smoke can
98 undergo chemical processing through photochemical and heterogeneous reactions, including the
99 loss of chloride and acquisition of sulfate and nitrate, creating potassium sulfate compounds in
100 smoke that are often used as tracers of aged smoke and can affect the hygroscopicity of smoke
101 particles (Capes et al., 2008; Hennigan et al., 2010, 2011; Reid et al., 2005; Zauscher et al.,
102 2013). The many variations and changes in the chemical and physical properties of smoke
103 particles during their residence time in the atmosphere makes it difficult to study these particles
104 thoroughly and can also affect their ability to act as CCN.

105 In this study, we investigated the relationship between submicron aerosol composition
106 and CCN in the tropical north Atlantic MBL during marine background conditions and
107 conditions affected by long-range continental aerosol transport (including dust and smoke). To
108 perform this work, we collected aerosol samples and size-resolved CCN data from January to
109 February 2020 at the Barbados Atmospheric Chemistry Observatory (BACO) during the
110 Elucidating the Role of Clouds–Circulation Coupling in Climate/Atlantic Tradewind Ocean-
111 Atmosphere Mesoscale Interaction Campaign (EUREC⁴A/ATOMIC) campaigns (Quinn et al.,
112 2021; Stevens et al., 2021). Conducting this research during the boreal winter provided a unique
113 opportunity to explore aerosol-cloud interactions in different meteorological conditions than are
114 typically studied in the tropical North Atlantic. Dust primarily arrives to Barbados during the
115 summer months with peaks in June and July (Zuidema et al., 2019). As a result, dust receptor
116 sites in Barbados have historically been used to compare dust and marine background conditions



117 during the boreal summer. During the winter, the southward shift of the ITCZ directs African
118 dust to South America, resulting in a decrease in dust concentrations over Barbados during the
119 winter months with days in December and January sometimes receiving no dust at all (Prospero,
120 1968; Prospero et al., 2014; Prospero & Lamb, 2003; Prospero & Mayol-Bracero, 2013). However,
121 during the EUREC⁴A/ATOMIC campaigns, we observed anomalous wintertime transport of
122 African aerosols to Barbados, which provided novel sampling conditions to study the effects of
123 various aerosol types on cloud droplet formation. Specifically, we were able to explore marine
124 aerosols such as organics, sulfates, and sea salt and how the addition of continental aerosols like
125 mineral dust and smoke particles affects CCN activity, thus comparing the impact of ocean-
126 derived vs. long-range transported aerosol on water uptake properties and CCN concentrations.
127 We conclude this manuscript by discussing the importance of our findings for cloud formation in
128 the tropical North Atlantic.

129 **Methods**

130 Measurement Site and Sampling Period

131 Aerosol samples and size-resolved CCN data were collected at the Barbados
132 Atmospheric Chemistry Observatory (BACO) on Ragged Point during the EUREC⁴A and
133 ATOMIC field campaigns from January 20, 2020 -February 20, 2020 (Quinn et al., 2021;
134 Stevens et al., 2021). Ragged Point (13° 6' N, 59° 37' W), a prominence on Barbados' east coast,
135 is an ideal location for studying the impact of long-range African aerosol transport on cloud-
136 aerosol interactions as it is situated on the most easterly island in the Caribbean and is exposed to
137 the steady easterly trade winds. Thus, the east coast of the island is subject to little anthropogenic
138 aerosol influence from local islands to the west (Prospero et al., 2005; Savoie et al., 2002).
139 Further, the island is at a latitude coinciding with the outflow of African aerosols such as mineral



140 dust (Carlson & Prospero, 1972; Prospero, 1968) and biomass burning (Archibald et al., 2015) as
141 well as tropical marine cumulus clouds (Stevens et al., 2016).

142 Air Mass Origins

143 During the sampling period, air masses of varying composition were observed at Ragged
144 Point. To determine the origin of these air masses, 150 h back trajectories were generated every 6
145 hours (h) at heights of 500, 1000, and 1500 meters (m) throughout the campaign using the
146 Hybrid Single Particle Lagrangian Integrated Trajectory (HYSPLIT) model calculated using
147 model vertical velocity and meteorology from the National Center for Environmental Prediction
148 (NCEP) 1-degree Global Data Assimilation System (GDAS) (Rolph et al., 2017; Stein et al.,
149 2015).

150 Dust Concentration

151 To collect aerosols, BACO is equipped with a high-volume sampler and an isokinetic
152 aerosol inlet on top of a 17 m tall tower situated on a 30 m bluff along the coast at Ragged Point.
153 Daily dust mass concentrations were determined from filter-based measurements (Prospero et al.,
154 2021; Zuidema et al., 2019) using a high-volume air sampler pumping at a rate of approximately
155 0.7 m³/min across a 20 cm x 25 cm cellulose Whatman-41 (W-41) filter. W-41 filters were
156 chosen for this analysis as they allow for high flow rates and yield a collection efficiency of 95%
157 or better for dust (Kitto & Anderson, 1988). Upper particle diameter limits for W-41 filters with 20
158 µm pore size are approximately 80-100 µm or greater (Barkley 2021). After aerosol collection,
159 the filters are placed in a furnace and combusted at 500°C for about 12 hrs. (i.e., overnight).
160 Procedural blanks are also collected by placing a filter in the sampler for 15 minutes without
161 turning on the pump. The resulting ash mass minus the mass of a filter blank is the approximate



162 amount of mineral dust collected on the filter during the sample period. A correction factor of 1.3
163 is applied to the calculated dust concentrations to account for dust components such as bound
164 water or soluble ions that are lost during the heating process (Prospero, 1999; Zuidema et al.,
165 2019).

166 Aerosol Chemical Composition

167 Aerosol particles were sampled at ambient relative humidity (RH) through an isokinetic
168 aerosol inlet and collected using a three-stage microanalysis particle sampler (MPS-3, California
169 Measurements, Inc.), which samples particles from diameters of 5.0-2.5 μm (stage 1), 2.5 μm –
170 0.7 μm (stage 2), and $<0.7 \mu\text{m}$ (stage 3). For each set of samples (1 set including 1 sample from
171 each stage of the MPS), the MPS was run for 45 min at 2 L/min flow starting at approximately
172 9:30 local time or 13:30 coordinated universal time (UTC). Meteorological data from a local
173 station was also used to manually check that wind direction fell between 335° and 130° and wind
174 speeds were greater than 1 m/s during all sampling periods. Sampling during these wind
175 conditions ensures that only air from the open ocean was sampled rather than local,
176 anthropogenically-influenced air.

177 Particles were deposited onto carbon-coated copper grids (Ted Pella, Inc.) that were
178 later analyzed at the Pacific Northwest National Laboratory using computer-controlled scanning
179 electron microscopy coupled with energy dispersive x-ray spectroscopy (CCSEM/EDX; Quanta
180 3D) to determine the elemental composition of individual particles. Here we focus only on the
181 submicron particle population which exerts a greater influence on CCN number concentrations
182 and is more sensitive to chemical changes that affects its hygroscopicity. Thus, for this study we
183 only present data from stage 3 of the MPS, representing $<0.7 \mu\text{m}$ diameter particles. Data for the
184 other stages will be the subject of a future manuscript.



185 EDX is considered a semiquantitative method providing the relative atomic fractions for
186 elements of interest. Percent composition threshold values of 1% were used to ensure the
187 presence of elements detected by the EDX. Elements of interest in CCSEM/EDX analysis were
188 limited to 16 common elements indicative of organic material, sea spray, dust, and anthropogenic
189 emissions: carbon (C), nitrogen (N), oxygen (O), sodium (Na), magnesium (Mg), aluminum (Al),
190 silicon (Si), phosphorus (P), sulfur (S), chlorine (Cl), potassium (K), calcium (Ca), vanadium
191 (V), manganese (Mn), iron (Fe), and nickel (Ni). The EDX peak for Cu is heavily influenced by
192 a background signal from the Cu grid and is excluded from analysis. Samples collected on Si
193 substrates confirmed the validity of the C signal in analyzed particles, as the carbon coating on
194 the Cu substrates has the potential to generate a background signal as well. An excess of 1000
195 particles were analyzed in each sample. Due to size limitations of the CCSEM, only particles
196 with diameters $>0.1 \mu\text{m}$ were analyzed. Data products from CCSEM/EDX analysis were then
197 analyzed in MATLAB (ver 9.6.0; The Mathworks, Inc.) using a K-means clustering algorithm
198 (Ault et al., 2012; Shen et al., 2016). The algorithm operates by generating categories of similar
199 particles (clusters) based on the presence and intensity of elemental peaks in individual single-
200 particle EDX spectra. These clusters are then assigned to particle types based on their size,
201 morphology, characteristic EDX spectra, and existing literature. Particle types typically observed
202 in the supermicron aerosol loading, such as sea salt and dust, are not as abundant in our samples
203 as we focus exclusively on the submicron aerosol loading.

204

205 Size-Resolved CCN Measurements and Data Analysis

206 To determine the size-resolved CCN activity of aerosol particles during the sampling
207 period, we used a continuous-flow streamwise thermal gradient CCN counter (CCNC, model



208 CCN-100, DMT, Longmont, Co, USA; (Roberts & Nenes, 2005; Rose et al., 2008)) combined with
209 a differential mobility analyzer (DMA, model M, Grimm Aerosol Technik, Ainring, Germany)
210 and condensation particle counter (CPC, model 5412, Grimm Aerosol Technik). Upon entering
211 the system, sampled air was dried using a condensation drier to maintain a relative humidity
212 (RH) between 20 and 30% and to ensure reliable hygroscopicity measurements. After drying,
213 particles passed through a DMA which selected particles with a diameter (D) between 20 and
214 245 nm. The monodisperse aerosol-laden flow was then split between the CCNC and CPC.
215 Inside the CCNC, particles were subjected to water vapor supersaturations (S) including 0.09,
216 0.16, 0.24, 0.43, and 0.74 %.

217 Calibrations of the CCNC supersaturations were performed according to the method
218 described in Rose et al., 2008 by generating and size-selecting ammonium sulfate particles that
219 were analyzed by the CCNC set to a designated temperature gradient as well as a CPC to
220 measure total condensation nuclei (CN) values. Plots comparing CCN/CN and dry particle
221 diameter were then used to determine the diameter at which 50% of the particles in an aerosol
222 population activate as CCN at a particular S, also called the critical activation diameter (d_{50}). D_{50}
223 values were then used to determine supersaturation. Supersaturations were plotted against the
224 designated temperature at the calculated supersaturation. The resulting plot provided a linear
225 curve that could be used to adjust the supersaturation shown by the instrument to the actual value
226 of the column supersaturation. After calibrating, S values averaged 0.08, 0.15, 0.23, 0.41, and
227 0.71.

228 For ambient sampling, particles that activate as CCN at each S and D are counted in the
229 CCNC as CCN, while all particles of a selected D are counted in the CPC to determine the total
230 aerosol concentration of particles at each D. By scanning D at a given value of S, measurements



231 from the CPC and CCNC are then used to calculate the d_{50} . These values, along with the particle
232 number size distribution determined by a scanning mobility particle sizer (SMPS, TSI model
233 3080 with CPC 3772) operating independently of the CCNC setup, are then used to calculate the
234 activation curve and the effective hygroscopicity parameter κ using equation (1) according to the
235 κ -Köhler model (Petters & Kreidenweis, 2007):

$$236 \quad \kappa = \frac{4A^3}{27D_p^3 \ln^2 S_{\text{crit}}} \quad (1)$$

237 where D_p is the dry particle diameter, S_{crit} is the supersaturation set by the CCN counter, and A is
238 the Kelvin term calculated from equation (2):

$$239 \quad A = \frac{4\sigma M_w}{RT\rho_w} \quad (2)$$

240 Where σ is the surface tension ($\sigma=0.072$ J/m²), R is the universal gas constant, M_w is the
241 molecular weight of water, and ρ_w is the density of water. In the κ -Köhler model, higher values
242 of κ indicate a more hygroscopic particle that is more efficient at taking up water and can
243 activate as CCN at lower S . Calculations of activation curves, size-resolved CCN, CCN
244 efficiencies, and errors are described in detail in Pöhlker et al., 2016.

245 **Results and Discussion**

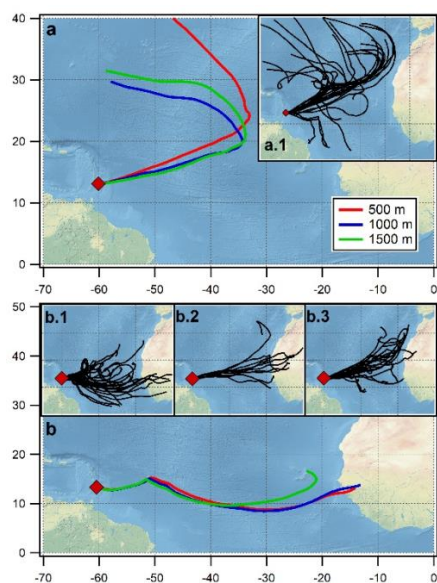
246 We find that, upon arrival of co-transported dust and smoke, smoke originating from fires
247 in the African Sahel dominate the accumulation mode particle population in the tropical North
248 Atlantic MBL, which results in an increase in CCN number concentration. Though dust and
249 smoke are both transported to the region, smoke dominates the accumulation mode number
250 concentration by an order of magnitude compared to dust. These findings are supported by data
251 products from dust mass concentrations, size-resolved hygroscopicity, single particle data (e.g.,



252 CCSEM-EDX), and air mass history (e.g., NOAA'S HYSPLIT model), which all complement
253 one another and provide unique insights into the aerosol sources, their single particle
254 composition, and their effects on cloud droplet activation.

255 Sampling Conditions during the EUREC⁴A and ATOMIC Campaigns

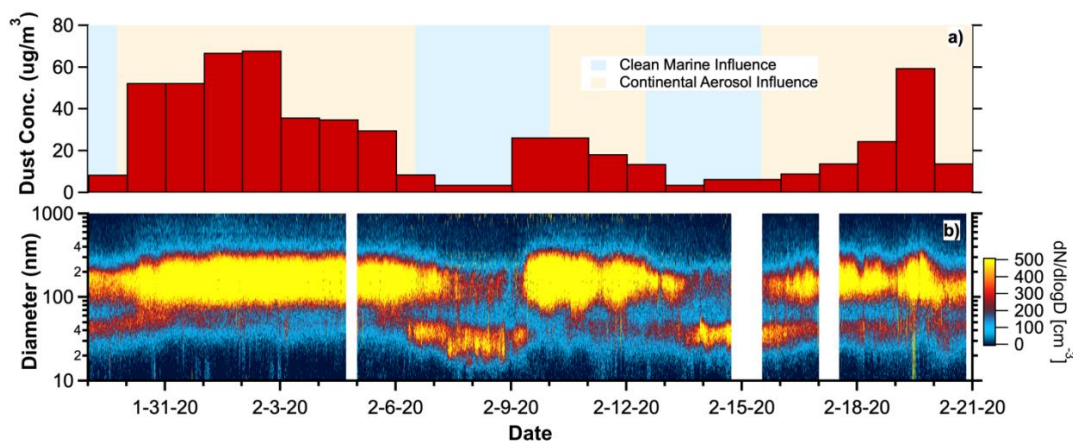
256 Barbados was influenced by two types of air masses during the sampling period: air
257 masses that do not pass over land (referred to as clean marine conditions), and air masses
258 influenced by continental regions (referred to as continental aerosol transport (CAT) events). To
259 confirm the origins of the various air masses sampled, we performed back trajectory analysis
260 throughout the campaign using NOAA'S HYSPLIT model. Figure 1 shows that during periods
261 with low dust mass concentrations and a bimodal size distribution, air masses originated from the
262 remote Atlantic Ocean at higher latitudes with no land contact over 6 days. During time periods
263 with high dust mass concentrations, air masses originated from continental Africa. Figure 2a
264 shows that the total mass concentration of dust particles correlates very well with the arrival of
265 air masses originating from Africa. During time periods when dust concentrations were low, the
266 particle loading has a bimodal size distribution characteristic of clean marine air masses (Figure
267 2b) (Hoppel et al., 1986). Upon the increase in dust mass concentrations, the submicron particle
268 size distribution correspondingly becomes unimodal and the smallest Aitken size mode is
269 negligible, suggesting that transported particles are overwhelming the background marine
270 particle loading or that smaller particles are coagulating onto larger transported continental
271 aerosols (Tomlin et al., 2021).



272

273 **Figure 1:** HYSPLIT back trajectories at Ragged Point, Barbados (red diamond) for the
274 EUREC⁴A/ATOMIC field campaign. (a) Back trajectories for 2020/2/8 18:00 UTC at heights of
275 500 m (red), 1000 m (blue), and 1500 m (green) exemplify air mass origins during clean marine
276 sampling conditions. Subplot a.1 shows all back trajectories from clean marine sampling
277 conditions collected at 6 h intervals with a release altitude of 1000 m from 2020/1/29 0:00 –
278 2020/1/29 12:00, 2020/2/6 12:00 – 2020/2/9 18:00 and 2020/2/12 12:00 – 2020/2/15 6:00 UTC.
279 (b) Back trajectories for 2020/2/2 18:00 UTC at 500 m, 1000 m, and 1500 m exemplify air mass
280 origins during continental sampling conditions. The subplots, b.1, b.2, and b.3 show all back
281 trajectories for 3 time periods during which continental aerosols were sampled, including
282 2020/1/29 18:00 – 2020/2/6 6:00, 2020/2/10 0:00 – 2020/2/12 6:00, and 2020/2/15 12:00 –
283 2020/2/20 18:00 UTC. Trajectories for b subplots were also collected at 6 h intervals with a
284 release altitude of 1000 m.

285



286

287 **Figure 2** – Temporal evolution of (a) dust mass concentrations determined from bulk aerosol
288 filter samples and (b) aerosol particle size distributions determined with an SMPS. Time for both
289 plots is given in UTC (-4 h local Atlantic Standard Time).

290

291 Single Particle Aerosol Composition

292 CCSEM/EDX analysis revealed the presence of several particle types in the submicron
293 aerosol loading with distinct morphologies and chemistries (Ault et al., 2014; Behnke et al.,
294 1997; Gaston et al., 2011a, 2013a) during the EUREC⁴A and ATOMIC campaigns. Figure 3
295 presents SEM images (left) and EDX spectra (right) for each particle type detected on stage 3 of
296 the MPS (particle diameter <0.7 μm), including aged sea spray, mineral dust, sulfate, smoke,
297 internally mixed dust and smoke, and organics. Sea spray was a dominant component of the
298 supermicron aerosol loading but is only a minor component of submicron aerosol.

299 *Aged Sea Spray*

300 Aged sea spray was defined by the presence of sea salt components including Na, Mg, K, S,
301 and Cl. In contrast to freshly emitted sea spray particles, aged sea spray has a characteristically



302 low or absent Cl signal with a strong presence of N or S. Sea spray can be aged through reactions
303 with sulfuric acid (H_2SO_4), dinitrogen pentoxide (N_2O_5), and/or nitric acid (HNO_3) which results
304 in Cl depletion and S or N enrichment (Ault et al., 2013, 2014; Behnke et al., 1997; Gaston et al.,
305 2011, 2013; Sobanska et al., 2003).

306 *Mineral Dust*

307 Mineral dust is characterized by the presence of aluminosilicate elements such as Si, Al, Fe,
308 K, Ca, and Mg in EDX spectra, which is consistent with previous studies of African dust
309 (Denjean et al., 2015; Hand et al., 2010; Levin et al., 2005; Twohy et al., 2009). Elements such
310 as S and N were not observed in this particle type (Kandler et al., 2018) suggesting that detected
311 dust did not undergo chemical processing during transport.

312

313 *Sulfate*

314 Sulfate-rich particles are a prevalent component of marine submicron aerosol (O'Dowd & de
315 Leeuw, 2007) and characterized here by a dominant S component - often with strong C, O, and N.
316 These particles are likely sulfates bound to NH_4^+ such as ammonium sulfate ($(\text{NH}_4)_2\text{SO}_4$) or
317 ammonium bisulfate (NH_4HSO_4) (Hand et al., 2010). The strong C component indicates a large
318 organic fraction as well.

319 *Smoke*

320 Smoke particles were identified by the presence of C with K and S likely representing
321 internally mixed organic and black carbon with potassium-containing salts. K is a well-known
322 indicator for biomass burning (Andreae, 1983; Hand et al., 2010; Hudson et al., 2004; Li et al.,



323 2003; Murphy et al., 2006; Pósfai et al., 2003), especially in flaming conditions in Savannah fires
324 as opposed to smoldering conditions (Echalar et al., 1995; Maenhaut et al., 1996).

325 Morphologically, smoke particles can be spherical due to aging or coating but can also appear as
326 aggregates or chains of spheroids (Dang et al., 2021; Hand et al., 2010; Miller et al., 2021; Pósfai
327 et al., 2003).

328 *Internally Mixed Dust and Smoke*

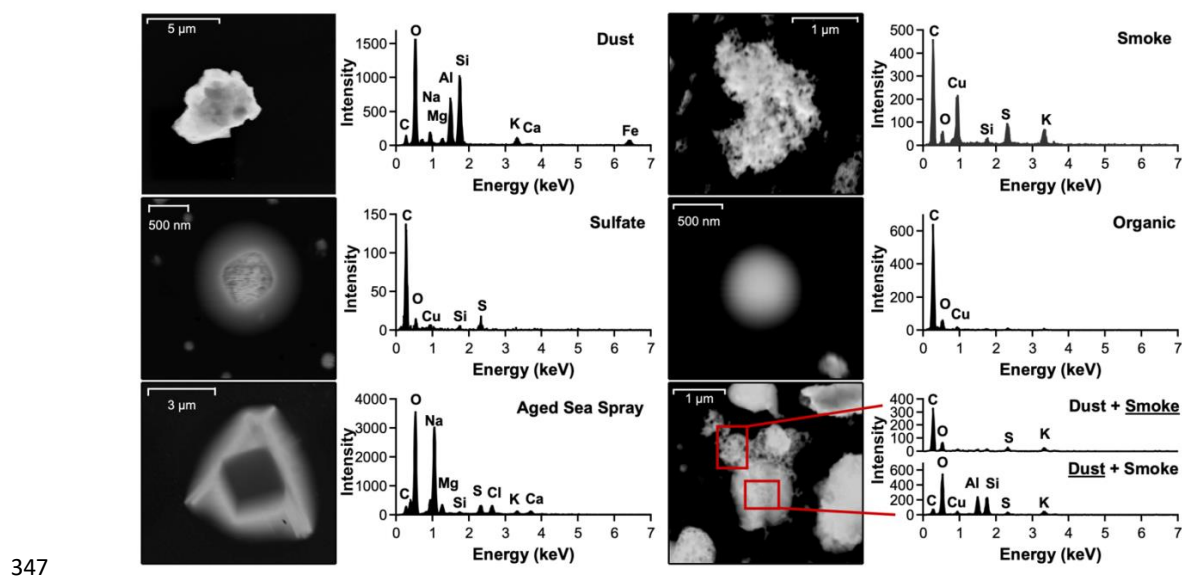
329 Internally mixed dust and smoke particles are characterized by dust components such as Si,
330 Al, Mg, Fe, Ca, and Mg with strong contributions of K, S, C, and O. Morphologically, internal
331 mixtures of dust and smoke appear as aggregates of amorphous dust particles with clusters or
332 spheres representing soot from smoke. Single particle chemical analysis of these particles shows
333 distinctions between the dust and smoke portion of the particle, with the dust portion having
334 typical dust components (Si, Al, Mg, Fe, Ca, and Mg) and the smoke portion having typical
335 smoke components (K and S with C and O). Previous research has observed internal mixing of
336 carbonaceous particles and dust particles in Africa when significant amounts of both biomass
337 burning and dust were present (Hand et al., 2010); however, we show that these internal mixtures
338 can be transported all the way to the Caribbean as well.

339 *Organics*

340 Organic particles are defined by strong signals of C and O with few other elements present, if
341 any (Hand et al., 2010). This scarcity of additional elements includes S and N that, if present,
342 would be indicative of sulfate and nitrate, respectively. Morphologically, organic particles are
343 characterized as small individual spheres. The organics were likely marine in origin (Russell et
344 al., 2010) as they were the smallest particle type observed both during clean marine conditions



345 and during long-range continental aerosol indicative of a “background” aerosol type (Russell et
346 al., 2010).



347
348 **Figure 3:** Characteristic aerosol particle types observed by means of SEM-EDX images (left)
349 and spectra (right) in samples collected during the EUREC⁴A/ATOMIC campaign. Plots for
350 Dust + Smoke particle type represent different areas analyzed on the particle with EDX, denoted
351 by the red boxes.

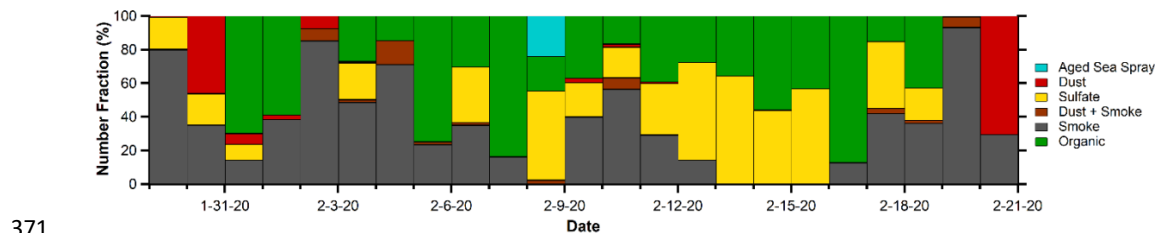
352

353 Arrival of Anomalous Wintertime Co-Transported Dust and Smoke

354 Figure 4 presents number fractions for particles detected in the submicron aerosol loading
355 throughout the sampling period and reveals a similar trend in smoke particle number fractions to
356 those of dust mass concentrations in Figure 2, suggesting that smoke and dust were co-
357 transported to Barbados from Africa. During the boreal winter, the Sahel region in North Africa
358 experiences its fire season in which large swathes of land are burned and large plumes of smoke



359 are emitted from the region (Figure S1;(Ansmann et al., 2009; Barkley et al., 2019; Roberts et
360 al., 2009). However, due to the southward shift in the ITCZ during the boreal winter, smoke is
361 expected to be transported primarily to South America (Moran-Zuloaga et al., 2018). In our
362 study, we observe the arrival of this smoke on Barbados. These findings are supported by
363 temporal carbon monoxide (CO) column density measurements that are often used as a tracer for
364 smoke (Figure S2 and S3). Periods that correspond to clean marine influence in the HYSPLIT
365 model from Figure 1 and low bulk dust mass concentrations in Figure 2 are dominated by sulfate
366 and organic particles in the submicron aerosol as exhibited in Figure 4. Upon arrival of
367 continental aerosols that correspond with continental aerosol influence from the HYSPLIT
368 model and bulk dust concentrations (2020/1/29 – 2020/2/7, 2020/2/9 – 2020/2/12 – 2020/2/16 –
369 2020/2/20 UTC), wildfire smoke appears to overwhelm the number fraction of the submicron
370 aerosol loading.



371

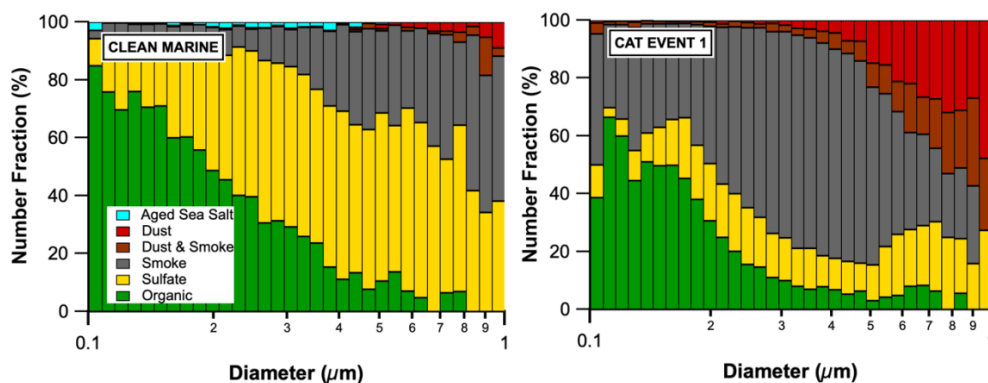
372 **Figure 4:** Temporal evolution of submicron number fractions for different types of aerosol
373 particles determined by CCSEM/EDX analysis. The total number of particles analyzed for each
374 day ranges from 1000 to 20,000.

375 Figure 5 provides a detailed size-resolved plot of single particle chemistry from both
376 clean marine periods (clean marine), and periods that were influenced by air masses from
377 continental Africa (CAT event 1). Analysis of other CAT events (Figure S4) show similar



378 chemical trends to those shown in the Cat Event 1 plot. Figure 5 shows that in both clean marine
379 periods and CAT events, a small fraction of large particles have both a smoke and a dust
380 signature. Both the clean marine and CAT event plot in Figure 5 demonstrate that dust and
381 internally mixed dust and smoke particles tend to be the largest particle types in the submicron
382 aerosol loading. This suggests that our clean marine conditions are “clean” compared to time
383 periods influenced by dust and smoke, rather than pristine clean marine conditions without any
384 continental aerosol influence. Smoke particles follow as the next largest particle type. The
385 smallest particle types were found to be organics followed by sulfates suggesting a primary
386 emission of marine organics and a secondary source for sulfate (Bates et al., 1992). Aged sea salt
387 particles were on average smaller than most dust, internally mixed dust and smoke, and smoke
388 particles. Figure 4 also shows that at a diameter of $\sim 0.1\mu\text{m}$ (which is approximately the d_{50} of
389 CCN at S 0.16% in clean marine and dusty conditions) the chemistry is dominated by sulfates
390 and organics in the clean marine conditions, while smoke and organics dominate in the CAT
391 event. A large decrease in sulfate number fraction suggests that marine biogenic sulfur
392 precursors are condensing onto larger transported particles and might explain the loss of the
393 Aitken mode observed in Figure 2.

394



395

396 **Figure 5:** Number fractions of different types of submicron aerosol particles plotted against
397 particle diameter. The “clean marine” plot (left) includes data from all clean marine sampling
398 periods. The “CAT Event 1” plot (right) includes data from the first period in which dust and
399 wildfire smoke were observed over Barbados (2020/1/29 18:00 – 2020/2/6 6:00 UTC). Bin sizes
400 for each decade can range from 34 particles to up to 3041 with an average bin size of 493
401 particles for the Clean Marine plot and 973 for the CAT Event plot.

402

403 Changes in Aerosol Hygroscopicity during EUREC⁴A/ATOMIC

404 Comparisons between size-resolved CCN measurements and submicron single particle
405 elemental composition reveal that smoke particles lower submicron aerosol hygroscopicity
406 compared to marine-derived submicron aerosol in the tropical North Atlantic. Figure 6 presents
407 boxplots for κ values as well as average d_{50} measured at each S during both clean marine
408 conditions and dusty conditions. Both plots show a similar trend in which average κ increases
409 from 0.09% S to 0.24% S. Then, with each subsequent increase in S after 0.24% S, κ decreases
410 likely due to smaller, less hygroscopic particles activating at higher supersaturations. Also of
411 note is the κ of 0.6 observed for clean marine conditions at 0.24% S, which matches κ



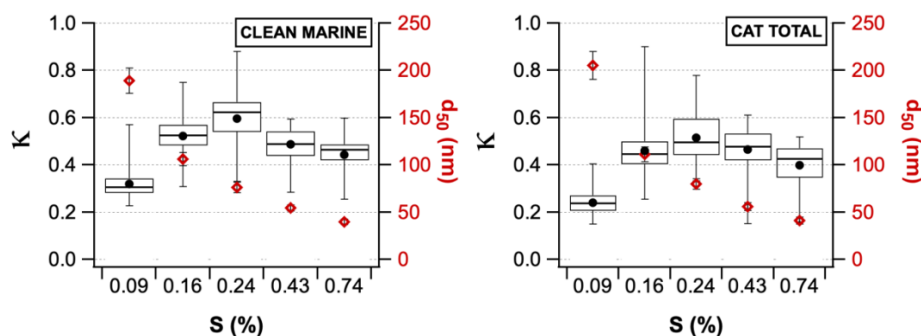
412 measurements for ammonium sulfate particles that can dominate along with sea spray organics
413 during clean marine conditions (Petters & Kreidenweis, 2007).

414 There is also a noticeable drop in average κ between the same supersaturations in clean
415 marine conditions compared to smokey conditions. For example, at 0.16% S, $\kappa=0.52\pm 0.09$ for
416 clean marine conditions and $\kappa=0.46\pm 0.10$ for continental aerosol transport. This is likely due to
417 the addition of less hygroscopic material such as dust and smoke particles that are acting as CCN
418 and are not present in clean marine conditions. As expected, trends in average d_{50} for both plots
419 show that activation diameters decrease with an increase in supersaturation, indicating that
420 smaller particles activate as CCN with larger supersaturations. Activation diameters during CAT
421 conditions are also larger than corresponding activation diameters in clean marine conditions for
422 the same supersaturation. This also suggests that the addition of less soluble material from
423 transported smoke particles lowers the hygroscopicity and increases the activation diameter.

424 When comparing hygroscopicity data from this study to previous research, we find both
425 similarities and differences in κ trends. For example, Good et al., 2010 presents data collected in
426 the tropical eastern Atlantic that provides an ideal comparison to our findings. On average, their
427 values for κ in clean marine conditions and during observations of dust transport ($\kappa=1.15-1.4$ and
428 $0.8-0.92$, respectively) were much higher than our observed values. However, one finding of note
429 from Good et al., 2010 is the distinct drop in κ between clean marine conditions and conditions
430 influenced by continental aerosols from Africa owing to the addition of more hydrophobic
431 particles such as dust that activate as CCN. Our data shows a similar drop in κ from clean marine
432 conditions to conditions influenced by long-range transported African aerosols. Wex et al., 2016
433 present ground-based field sampling of CCN data in November and April at Ragged Point,
434 Barbados. They show a similar trend in κ in which values increase from 0.1% S, peak at 0.2% S,



435 then decrease with each subsequent increase in S . Wex et al., 2016 also found a similar drop in κ
436 upon the arrival of long-range transported aerosols, likely due to less hygroscopic particles from
437 continental sources activating as CCN. A separate study from Kristensen et al., 2016 conducted
438 similar research at Ragged Point, Barbados during the boreal summer. The range in κ values of
439 0.2-0.5 match those observed in our work, especially during CAT events. However, Kristensen et
440 al., 2016 determined that concentrations of dust, sea salt, and soot were too small to influence
441 CCN, concluding that sulfates and organics were the primary CCN types. We find this is the case
442 for clean marine conditions but the change in κ between clean marine and CAT events indicates
443 the influence of an additional CCN particle type.



444

445 **Figure 6:** Hygroscopicity parameter κ (left axis, box plots) and corresponding mean critical
446 diameter “ d_{50} ” (right axis; red markers) for the investigated levels of water vapor supersaturation
447 (S). Black dots in the boxplot indicate κ mean values.

448

449

450 African Smoke Particles Enhance CCN Concentrations

451

452 Comparisons between smoke fractions and CCN counts suggest that smoke particles
enhance the number of CCN in the tropical N Atlantic MBL. Figure 7 presents two temporal

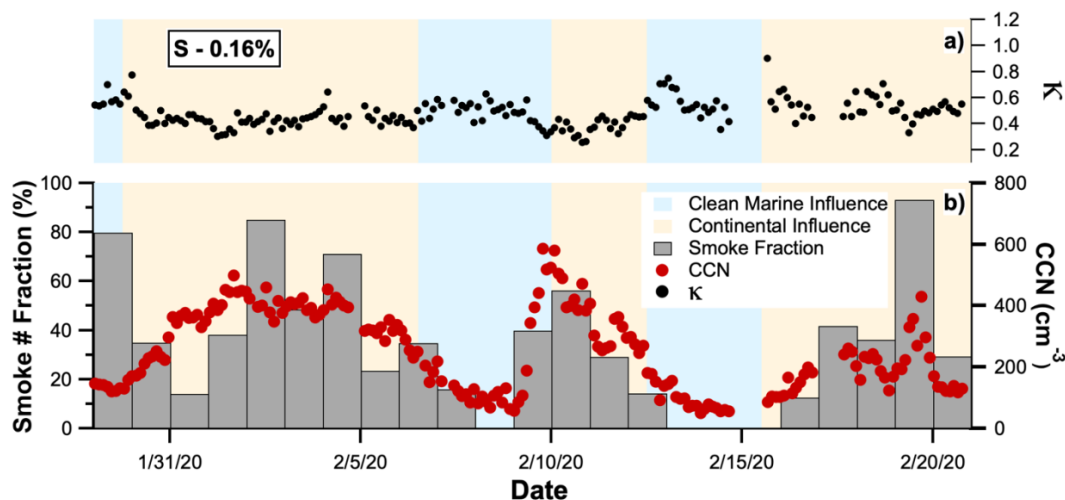


453 plots of κ (Figure 7a) and smoke number fractions with CCN counts measured at 0.16% S
454 (Figure 7b). Table 1 provides averages of CCN concentrations for each time period shown in
455 Figure 7b. Fig 7a suggests that there is an inverse relationship between κ and smoke number
456 fractions in which an increase in smoke particles results in a decrease in κ . This is likely due to
457 the activation of smoke particles as CCN, which are on average less hygroscopic than the sulfate
458 particles that act as CCN during clean marine conditions. In Fig 7b, there is a clear and direct
459 relationship between smoke number fractions and CCN counts.

460 There are several possible explanations for why African smoke particles may act as CCN.
461 As shown in Figure 5, smoke particles are larger than organics and sulfates, on average, and
462 overwhelm sulfate and organic particle number concentrations upon arrival of long-range
463 transported African aerosols. In this case, the relatively large size of the smoke particles makes
464 for better CCN compared to organics or sulfates via the Kelvin effect (Dusek et al., 2006). The
465 large number of smoke particles overwhelms the particle loading, providing more surface area
466 for water condensation than is available on sulfate or organic particles. Another potential
467 explanation for smoke particles acting as CCN could be the presence of water-soluble organic
468 compounds (WSOC) such as dicarboxylic acids and humic-like substances that increase CCN
469 numbers through the Raoult effect (Roberts et al., 2002). In addition to WSOC, aerosols can also
470 contain organic surfactants that decrease surface tension and thus lower the vapor pressure
471 necessary for CCN activation (Asa-Awuku et al., 2008; Facchini et al., 1999; Ovadnevaite et al.,
472 2017). Aging of organic components can also potentially explain the ability of smoke particles to
473 activate as CCN. Studies conducted on the aging of organic components show that a higher O:C
474 ratio (a proxy for aerosol organic aging) increases aerosol hygroscopicity (Jimenez et al., 2009;
475 Massoli et al., 2010). The long-range transport of smoke particles from Africa to Barbados



476 would theoretically provide ample exposure time of smoke particles to oxidants such that aging
477 of the particles could occur (Jimenez et al., 2009; Massoli et al., 2010). However, studies
478 exploring the aging of biomass burning particles specifically show that aging results in a drop in
479 κ , rather than an increase as observed in aging of secondary organic aerosols (Engelhart et al.,
480 2012). Finally, the presence of salts in smoke particles has been shown to be an important
481 component in smoke hygroscopicity and may explain why smoke is efficient as CCN. Previous
482 studies have shown that smoke particles often contain hygroscopic salts such as potassium
483 chloride, sulfate, and nitrate (e.g., KCl, KNO₃, and K₂SO₄) (Freney et al., 2009; Zauscher et al.,
484 2013). Other research also shows that only small fractions of salts are needed to increase aerosol
485 hygroscopicity (Roberts et al., 2002). It is likely that biomass burning hygroscopicity can be
486 explained by a combination of factors. For example, previous research has found that the
487 presence of salts can enhance the surfactant effect of hydrophobic organic compounds (Asa-
488 Awuku et al., 2008).



489

490 **Figure 7:** Temporal evolution of hygroscopicity parameter κ (black dots, upper panel) and CCN
 491 number concentration (red dots, lower panel), both measured at $S = 0.16\%$, and smoke particle
 492 number fraction (grey bars, left axis, lower panel). Background color shadings indicate periods
 493 of continental influence (orange) and clean marine influence (blue) determined by HYSPLIT
 494 back trajectories and dust mass concentrations.

495 **Table 1** – Values for average CCN Concentrations and κ measured at 0.16% S during each clean
 496 marine influence period and CAT event sampled during the EUREC⁴A and ATOMIC
 497 campaigns.

Sampling Period	Day/Time	CCN Concentrations (pt/cm ³)	Average κ
Clean Marine Period 1	2020/1/29:00 – 2020/1/29 12:00	140 \pm 10	0.58 \pm 0.07
CAT Event 1	2020/1/29 18:00 – 2020/2/6 6:00	340 \pm 90	0.44 \pm 0.08
Clean Marine Period 2	2020/2/6 12:00 – 2020/2/9 18:00	150 \pm 98	0.50 \pm 0.10
CAT Event 2	2020/2/10 0:00 – 2020/2/12 6:00	400 \pm 106	0.38 \pm 0.06
Clean Marine Period 3	2020/2/12 12:00 – 2020/2/15 6:00	100 \pm 42	0.55 \pm 0.10



CAT Event 3	2020/2/15 12:00 – 2020/2/20 – 18:00	190 \pm 75	0.54 \pm 0.10
-------------	-------------------------------------	--------------	-----------------

498

499 **Conclusions**

500 During clean marine conditions, the submicron aerosol loading consists primarily of
501 sulfate and organic particles. CCN measurements determine cloud activation by particles
502 approximately 80 nm in activation diameter with an average $\kappa = 0.52 \pm 0.08$. Comparisons
503 between particle size, hygroscopicity, and single particle elemental composition suggest that
504 sulfate particles (likely ammonium sulfate) are the primary CCN particles in clean marine
505 conditions. During the EUREC⁴A/ATOMIC campaign, Barbados received three African aerosol
506 transport events during which we detected mineral dust and smoke particles from northern
507 Africa. Upon the arrival of African aerosols to BACO, CCN average activation diameter
508 increased to approximately 200 nm while the average hygroscopicity of activated particles for all
509 CAT events decreased to $\kappa = 0.45 \pm 0.1$. Upon arrival of high concentrations of smoke particles to
510 Barbados, smoke particles overwhelm the accumulation mode particle loading, decrease aerosol
511 hygroscopicity, and also increase CCN number concentrations, which could also increase the
512 cloud droplet number concentration and alter cloud radiative properties (Twomey, 1974).
513 Overall, we find that smoke has a larger effect on CCN number concentrations than dust.

514 The observation of smoke transported to Barbados during the boreal winter also indicates
515 the large geographic extent of African smoke that can impact the MBL. Building upon recent
516 work from Ragged Point and other parts of the tropical and subtropical Atlantic (Holanda et al.,
517 2020; Kacarab et al., 2020; Schill et al., 2020; Zuidema et al., 2018) this work also indicates a
518 need for greater consideration of the impacts of smoke in the MBL. Previous research conducted
519 at Ragged Point has primarily focused on African dust, which reaches its maximum during the



520 boreal summer when smoke transport is low (Zuidema et al., 2019). To better contextualize our
521 findings, we analysed carbon monoxide column density (a tracer for smoke) as well as aerosol
522 optical depth (AOD) and aerosol optical thickness (AOT) (tracers for dust) from 2018-2022
523 (Figure S2 and S3). Figure S2 shows the temporal trends while Figure S3 show seasonal
524 averages. As expected, AOD and AOT peak in July when dust transport reaches a maximum.
525 However, Figures S2 and S3 indicate that smoke is decoupled from dust, reaching a maximum in
526 the spring around April and a minimum in the summer when dust transport is highest. This
527 finding suggests that while the dust transport during the EUREC4A/ATOMIC campaigns is
528 higher than average dust loadings during this month (Zuidema et al., 2019), the amount of smoke
529 observed is not unique, but rather characteristic of the region. Thus, smoke may be playing an
530 important role on CCN formation throughout a large portion of the year. This is especially true
531 considering the large size of long-range transported smoke plumes that have a wide geographic
532 extent in which they can affect cloud formation. To conclude, this work highlights the need to
533 characterize African smoke transport to Ragged Point and better understand the role of smoke in
534 cloud formation, radiative forcing, and climate (Pechony & Shindell, 2010; Shindell et al., 2009).

535 **Data Availability**

536 The data will be made publically available in the University of Miami data repository and will be
537 linked with a doi.

538 **Author Contributions**

539 Conceptualization of this work was done by HMR, MLP, OK, and CJG. Collection of samples
540 was conducted by HMR, OK, EB, and PS, while analysis was done by HMR, MLP, OK,>NNL,
541 and ZC. The development of the methods used in this work was done by HMR, MLP, OK, ZC,
542 SC, APA, and CJG. Instrumentation used to conduct this work were provided by MLP, SC,
543 APA, and CJG. Formal analysis of data was performed by HMR, MLP, CP, and OK. Validation
544 of data products was performed by HMR, ZC, SC, APA, and CJG. Computer code used for data
545 analysis was provided by MLP, OK, and APA. Data visualization was performed by HMR,
546 MLP, and OK. PKQ, PZ, CP, and UP helped interpret results. Supervision and project



547 administration duties were done by MLP and CJG. HMR wrote the original draft for publication,
548 and all co-authors reviewed and edited this work.

549 **Competing Interests**

550 Some authors are members of the editorial board of Atmospheric Chemistry and Physics. The
551 peer-review process was guided by an independent editor, and the authors have no other
552 competing interests to declare

553

554 **Acknowledgements**

555 C.J.G. acknowledges an NSF CAREER award (1944958). A portion of this research was
556 performed on project awards (10.46936/lser.proj.2019.50816/60000110 and
557 10.46936/lser.proj.2021.51900/60000361) from the Environmental Molecular Sciences
558 Laboratory, a DOE Office of Science User Facility sponsored by the Biological and
559 Environmental Research program under Contract No. DE-AC05-76RL01830. P.K.Q.
560 acknowledges PMEL contribution number 5353. MLP and CP acknowledge support by the Max
561 Planck Society.

562

563

564

565

566

567

568

569

570 **References**

571 Adams, A. M., Prospero, J. M., & Zhang, C. (2012). CALIPSO-Derived Three-Dimensional Structure of
572 Aerosol over the Atlantic Basin and Adjacent Continents. *Journal of Climate*, 25, 6862–6879.



- 573 Albrecht, B. A. (1989). Aerosols, cloud microphysics, and fractional cloudiness. *Science*, 245(4923),
574 1227–1230. <https://doi.org/10.1126/science.245.4923.1227>
- 575 Allan, J. D., Baumgardner, D., Raga, G. B., Mayol-Bracero, O. L., Morales-García, F., García-García, F.,
576 Montero-Martínez, G., Borrmann, S., Schneider, J., Mertes, S., Walter, S., Gysel, M., Dusek, U.,
577 Frank, G. P., & Krämer, M. (2008). Clouds and aerosols in Puerto Rico – a new evaluation.
578 *Atmospheric Chemistry and Physics*, 8(5), 1293–1309. <https://doi.org/10.5194/acp-8-1293-2008>
- 579 Andreae, M. O. (1983). Soot Carbon and Excess Fine Potassium: Long-Range Transport of Combustion-
580 Derived Aerosols. *Science*, 220(4602), 1148–1151. <https://doi.org/10.1126/science.220.4602.1148>
- 581 Andreae, M. O. (2019). Emission of trace gases and aerosols from biomass burning -- an updated
582 assessment. *Atmospheric Chemistry and Physics*, 19(13), 8523–8546. <https://doi.org/10.5194/acp-19-8523-2019>
- 584 Ansmann, A., Baars, H., Tesche, M., Müller, D., Althausen, D., Engelmann, R., Pauliquevis, T., &
585 Artaxo, P. (2009). Dust and smoke transport from Africa to South America: Lidar profiling over
586 Cape Verde and the Amazon rainforest. *Geophysical Research Letters*, 36(11).
587 <https://doi.org/https://doi.org/10.1029/2009GL037923>
- 588 Archibald, A. T., Witham, C. S., Ashfold, M. J., Manning, A. J., O'Doherty, S., Grealley, B. R., Young,
589 D., & Shallcross, D. E. (2015). Long-term high frequency measurements of ethane, benzene and
590 methyl chloride at Ragged Point, Barbados: Identification of long-range transport events. *Elementa:
591 Science of the Anthropocene*, 3. <https://doi.org/10.12952/journal.elementa.000068>
- 592 Asa-Awuku, A., Sullivan, A. P., Hennigan, C. J., Weber, R. J., & Nenes, A. (2008). Investigation of
593 molar volume and surfactant characteristics of water-soluble organic compounds in biomass burning
594 aerosol. *Atmos. Chem. Phys.*, 8(4), 799–812. <https://doi.org/10.5194/acp-8-799-2008>
- 595 Ault, A. P., Guasco, T. L., Baltrusaitis, J., Ryder, O. S., Trueblood, J. v., Collins, D. B., Ruppel, M. J.,
596 Cuadra-Rodriguez, L. A., Prather, K. A., & Grassian, V. H. (2014). Heterogeneous Reactivity of
597 Nitric Acid with Nascent Sea Spray Aerosol: Large Differences Observed between and within
598 Individual Particles. *The Journal of Physical Chemistry Letters*, 5(15), 2493–2500.
599 <https://doi.org/10.1021/jz5008802>
- 600 Ault, A. P., Guasco, T. L., Ryder, O. S., Baltrusaitis, J., Cuadra-Rodriguez, L. A., Collins, D. B., Ruppel,
601 M. J., Bertram, T. H., Prather, K. A., & Grassian, V. H. (2013). Inside versus outside: Ion
602 redistribution in nitric acid reacted sea spray aerosol particles as determined by single particle
603 analysis. *Journal of the American Chemical Society*, 135(39), 14528–14531.
604 <https://doi.org/10.1021/ja407117x>
- 605 Ault, A. P., Peters, T. M., Sawvel, E. J., Casuccio, G. S., Willis, R. D., Norris, G. A., & Grassian, V. H.
606 (2012). Single-Particle SEM-EDX Analysis of Iron-Containing Coarse Particulate Matter in an
607 Urban Environment: Sources and Distribution of Iron within Cleveland, Ohio. *Environmental
608 Science & Technology*, 46(8), 4331–4339. <https://doi.org/10.1021/es204006k>
- 609 Barkley, A. E., Prospero, J. M., Mahowald, N., Hamilton, D. S., Pependorf, K. J., Oehlert, A. M.,
610 Pourmand, A., Gatineau, A., Panechou-Pulcherie, K., Blackwelder, P., & Gaston, C. J. (2019).
611 African biomass burning is a substantial source of phosphorus deposition to the Amazon, Tropical
612 Atlantic Ocean, and Southern Ocean. *Proceedings of the National Academy of Sciences*, 116(33),
613 16216 LP – 16221. <https://doi.org/10.1073/pnas.1906091116>



- 614 Bates, T. S., Lamb, B. K., Guenther, A., Dignon, J., & Stoiber, R. E. (1992). Sulfur emissions to the
615 atmosphere from natural sources. *Journal of Atmospheric Chemistry*, 14(1), 315–337.
616 <https://doi.org/10.1007/BF00115242>
- 617 Behnke, W., George, C., Scheer, V., & Zetzsch, C. (1997). Production and decay of ClNO₂ from the
618 reaction of gaseous N₂O₅ with NaCl solution: Bulk and aerosol experiments. *Journal of*
619 *Geophysical Research Atmospheres*, 102(3), 3795–3804. <https://doi.org/10.1029/96jd03057>
- 620 Behrenfeld, M. J., Moore, R. H., Hostetler, C. A., Graff, J., Gaube, P., Russell, L. M., Chen, G., Doney,
621 S. C., Giovannoni, S., Liu, H., Proctor, C., Bolaños, L. M., Baetge, N., Davie-Martin, C., Westberry,
622 T. K., Bates, T. S., Bell, T. G., Bidle, K. D., Boss, E. S., ... Ziemba, L. (2019). The North Atlantic
623 Aerosol and Marine Ecosystem Study (NAAMES): Science Motive and Mission Overview . In
624 *Frontiers in Marine Science* (Vol. 6). <https://www.frontiersin.org/article/10.3389/fmars.2019.00122>
- 625 Capes, G., Johnson, B., McFiggans, G., Williams, P. I., Haywood, J., & Coe, H. (2008). Aging of
626 biomass burning aerosols over West Africa: Aircraft measurements of chemical composition,
627 microphysical properties, and emission ratios. *Journal of Geophysical Research (Atmospheres)*,
628 113(D23), D00C15. <https://doi.org/10.1029/2008JD009845>
- 629 Carlson, T. N., & Prospero, J. M. (1972). The Large-Scale Movement of Saharan Air Outbreaks over the
630 Northern Equatorial Atlantic. *Journal of Applied Meteorology and Climatology*, 11(2), 283–297.
631 [https://doi.org/10.1175/1520-0450\(1972\)011<0283:TLSMOS>2.0.CO;2](https://doi.org/10.1175/1520-0450(1972)011<0283:TLSMOS>2.0.CO;2)
- 632 Carslaw, K. S., Lee, L. A., Reddington, C. L., Pringle, K. J., Rap, A., Forster, P. M., Mann, G. W.,
633 Spracklen, D. v, Woodhouse, M. T., Regayre, L. A., & Pierce, J. R. (2013). Large contribution of
634 natural aerosols to uncertainty in indirect forcing. *Nature*, 503(7474), 67–71.
635 <https://doi.org/10.1038/nature12674>
- 636 Chin, M., Diehl, T., Tan, Q., Prospero, J. M., Kahn, R. A., Remer, L. A., Yu, H., Sayer, A. M., Bian, H.,
637 Geogdzhayev, I. v, Holben, B. N., Howell, S. G., Huebert, B. J., Hsu, N. C., Kim, D., Kucsera, T.
638 L., Levy, R. C., Mishchenko, M. I., Pan, X., ... Zhao, X.-P. (2014). Multi-decadal aerosol variations
639 from 1980 to 2009: a perspective from observations and a global model. *Atmospheric Chemistry and*
640 *Physics*, 14(7), 3657–3690. <https://doi.org/10.5194/acp-14-3657-2014>
- 641 Dang, C., Segal-Rozenhaimer, M., Che, H., Zhang, L., Formenti, P., Taylor, J., Dobracki, A., Purdue, S.,
642 Wong, P.-S., Nenes, A., Sedlacek, A., Coe, H., Redemann, J., Zuidema, P., & Haywood, J. (2021).
643 Biomass burning and marine aerosol processing over the southeast Atlantic Ocean: A TEM single
644 particle analysis. *Atmos. Chem. Phys. Discuss.*, 2021, 1–30. <https://doi.org/10.5194/acp-2021-724>
- 645 Denjean, C., Caqueneau, S., Desboeufs, K., Laurent, B., Maille, M., Quiñones Rosado, M., Vallejo, P.,
646 Mayol-Bracero, O. L., & Formenti, P. (2015). Long-range transport across the Atlantic in
647 summertime does not enhance the hygroscopicity of African mineral dust. *Geophysical Research*
648 *Letters*, 42(18), 7835–7843. <https://doi.org/https://doi.org/10.1002/2015GL065693>
- 649 Dusek, U., Frank, G. P., Hildebrandt, L., Curtius, J., Schneider, J., Walter, S., Chand, D., Drewnick, F.,
650 Hings, S., Jung, D., Borrmann, S., & Andreae, M. O. (2006). Size Matters More Than Chemistry for
651 Cloud-Nucleating Ability of Aerosol Particles. *Science*, 312(5778), 1375–1378.
652 <https://doi.org/10.1126/science.1125261>



- 653 Echalar, F., Gaudichet, A., Cachier, H., & Artaxo, P. (1995). Aerosol emissions by tropical forest and
654 savanna biomass burning: Characteristic trace elements and fluxes. *Geophysical Research Letters*,
655 22(22), 3039–3042. <https://doi.org/https://doi.org/10.1029/95GL03170>
- 656 Edwards, E.-L., Corral, A. F., Dadashazar, H., Barkley, A. E., Gaston, C. J., Zuidema, P., & Sorooshian,
657 A. (2021). Impact of various air mass types on cloud condensation nuclei concentrations along
658 coastal southeast Florida. *Atmospheric Environment*, 254, 118371.
659 <https://doi.org/https://doi.org/10.1016/j.atmosenv.2021.118371>
- 660 Engelhart, G. J., Hennigan, C. J., Miracolo, M. A., Robinson, A. L., & Pandis, S. N. (2012). Cloud
661 condensation nuclei activity of fresh primary and aged biomass burning aerosol. *Atmospheric
662 Chemistry and Physics*, 12(15), 7285–7293. <https://doi.org/10.5194/acp-12-7285-2012>
- 663 Facchini, M. C., Mircea, M., Fuzzi, S., & Charlson, R. J. (1999). Cloud albedo enhancement by surface-
664 active organic solutes in growing droplets. *Nature*, 401(6750), 257–259.
665 <https://doi.org/10.1038/45758>
- 666 Forster, P., Storelvmo, T., Armour, K., William, C., Dufresne, J.-L., Frame, D., Lunt, D., Mauritsen, T.,
667 Palmer, M., Watanabe, M., Wild, M., & Zhang, H. (2021). Chapter 7: The Earth’s energy budget,
668 climate feedbacks, and climate sensitivity. *Climate Change 2021: The Physical Science Basis,
669 Contributi.*
- 670 Freney, E. J., Martin, S. T., & Buseck, P. R. (2009). Deliquescence and efflorescence of potassium salts
671 relevant to biomass-burning aerosol particles. *Aerosol Science and Technology*, 43(8), 799–807.
672 <https://doi.org/10.1080/02786820902946620>
- 673 Gaston, C. J., Furutani, H., Guazzotti, S. A., Coffee, K. R., Bates, T. S., Quinn, P. K., Aluwihare, L. I.,
674 Mitchell, B. G., & Prather, K. A. (2011). Unique ocean-derived particles serve as a proxy for
675 changes in ocean chemistry. *Journal of Geophysical Research Atmospheres*, 116(18), 1–13.
676 <https://doi.org/10.1029/2010JD015289>
- 677 Gaston, C. J., Quinn, P. K., Bates, T. S., Gilman, J. B., Bon, D. M., Kuster, W. C., & Prather, K. A.
678 (2013). The impact of shipping, agricultural, and urban emissions on single particle chemistry
679 observed aboard the R/V Atlantis during CalNex. *Journal of Geophysical Research Atmospheres*,
680 118(10), 5003–5017. <https://doi.org/10.1002/jgrd.50427>
- 681 Good, N., Topping, D. O., Allan, J. D., Flynn, M., Fuentes, E., Irwin, M., Williams, P. I., Coe, H., &
682 McFiggans, G. (2010). Consistency between parameterisations of aerosol hygroscopicity and CCN
683 activity during the RHaMBLe discovery cruise. *Atmos. Chem. Phys.*, 10(7), 3189–3203.
684 <https://doi.org/10.5194/acp-10-3189-2010>
- 685 Hand, V. L., Capes, G., Vaughan, D. J., Formenti, P., Haywood, J. M., & Coe, H. (2010). Evidence of
686 internal mixing of African dust and biomass burning particles by individual particle analysis using
687 electron beam techniques. *Journal of Geophysical Research: Atmospheres*, 115(D13).
688 <https://doi.org/https://doi.org/10.1029/2009JD012938>
- 689 Hennigan, C. J., Miracolo, M. A., Engelhart, G. J., May, A. A., Presto, A. A., Lee, T., Sullivan, A. P.,
690 McMeeking, G. R., Coe, H., Wold, C. E., Hao, W.-M., Gilman, J. B., Kuster, W. C., de Gouw, J.,
691 Schichtel, B. A., Collett Jr., J. L., Kreidenweis, S. M., & Robinson, A. L. (2011). Chemical and
692 physical transformations of organic aerosol from the photo-oxidation of open biomass burning



- 693 emissions in an environmental chamber. *Atmospheric Chemistry and Physics*, 11(15), 7669–7686.
694 <https://doi.org/10.5194/acp-11-7669-2011>
- 695 Hennigan, C. J., Sullivan, A. P., Collett Jr., J. L., & Robinson, A. L. (2010). Levoglucosan stability in
696 biomass burning particles exposed to hydroxyl radicals. *Geophysical Research Letters*, 37(9).
697 <https://doi.org/https://doi.org/10.1029/2010GL043088>
- 698 Holanda, B. A., Pöhlker, M. L., Walter, D., Saturno, J., Sörgel, M., Ditas, J., Ditas, F., Schulz, C., Franco,
699 M. A., Wang, Q., Donth, T., Artaxo, P., Barbosa, H. M. J., Borrmann, S., Braga, R., Brito, J.,
700 Cheng, Y., Dollner, M., Kaiser, J. W., ... Pöhlker, C. (2020). Influx of African biomass burning
701 aerosol during the Amazonian dry season through layered transatlantic transport of black carbon-
702 rich smoke. *Atmospheric Chemistry and Physics*, 20(8), 4757–4785. <https://doi.org/10.5194/acp-20-4757-2020>
- 704 Hoppel, W. A., Frick, G. M., & Larson, R. E. (1986). Effect of nonprecipitating clouds on the aerosol size
705 distribution in the marine boundary layer. *Geophysical Research Letters*, 13(2), 125–128.
706 <https://doi.org/https://doi.org/10.1029/GL013i002p00125>
- 707 Hudson, P. K., Murphy, D. M., Cziczo, D. J., Thomson, D. S., de Gouw, J. A., Warneke, C., Holloway, J.,
708 Jost, H.-J., & Hübler, G. (2004). Biomass-burning particle measurements: Characteristic
709 composition and chemical processing. *Journal of Geophysical Research: Atmospheres*, 109(D23).
710 <https://doi.org/https://doi.org/10.1029/2003JD004398>
- 711 Jimenez, J. L., Canagaratna, M. R., Donahue, N. M., Prevot, A. S. H., Zhang, Q., Kroll, J. H., DeCarlo, P.
712 F., Allan, J. D., Coe, H., Ng, N. L., Aiken, A. C., Docherty, K. S., Ulbrich, I. M., Grieshop, A. P.,
713 Robinson, A. L., Duplissy, J., Smith, J. D., Wilson, K. R., Lanz, V. A., ... Worsnop, D. R. (2009).
714 Evolution of organic aerosols in the atmosphere. *Science*, 326(5959), 1525–1529.
715 <https://doi.org/10.1126/science.1180353>
- 716 Kacarab, M., Thornhill, K. L., Dobracki, A., Howell, S. G., O'Brien, J. R., Freitag, S., Poellot, M. R.,
717 Wood, R., Zuidema, P., Redemann, J., & Nenes, A. (2020). Biomass burning aerosol as a modulator
718 of the droplet number in the southeast Atlantic region. *Atmos. Chem. Phys.*, 20(5), 3029–3040.
719 <https://doi.org/10.5194/acp-20-3029-2020>
- 720 Kitto, M. E., & Anderson, D. L. (1988). The use of Whatman-41 filters for particle. *Atmospheric*
721 *Environment (1967)*, 22(11), 2629–2630. [https://doi.org/https://doi.org/10.1016/0004-6981\(88\)90500-8](https://doi.org/https://doi.org/10.1016/0004-6981(88)90500-8)
- 723 Klingebiel, M., Ghate, V. P., Naumann, A. K., Ditas, F., Pöhlker, M. L., Pöhlker, C., Kandler, K.,
724 Konow, H., & Stevens, B. (2019). Remote Sensing of Sea Salt Aerosol below Trade Wind Clouds.
725 *Journal of the Atmospheric Sciences*, 76(5), 1189–1202. <https://doi.org/10.1175/JAS-D-18-0139.1>
- 726 Kristensen, T. B., Müller, T., Kandler, K., Benker, N., Hartmann, M., Prospero, J. M., Wiedensohler, A.,
727 & Stratmann, F. (2016). Properties of cloud condensation nuclei (CCN) in the trade wind marine
728 boundary layer of the western North Atlantic. *Atmos. Chem. Phys.*, 16(4), 2675–2688.
729 <https://doi.org/10.5194/acp-16-2675-2016>
- 730 Latham, T. L., Beyersdorf, A. J., Thornhill, K. L., Winstead, E. L., Cubison, M. J., Hecobian, A.,
731 Jimenez, J. L., Weber, R. J., Anderson, B. E., & Nenes, A. (2013). Analysis of CCN activity of
732 Arctic aerosol and Canadian biomass burning during summer 2008. *Atmospheric Chemistry and*
733 *Physics*, 13(5), 2735–2756. <https://doi.org/10.5194/acp-13-2735-2013>



- 734 Levin, Z., Teller, A., Ganor, E., & Yin, Y. (2005). On the interactions of mineral dust, sea-salt particles,
735 and clouds: A measurement and modeling study from the Mediterranean Israeli Dust Experiment
736 campaign. *Journal of Geophysical Research: Atmospheres*, 110(D20).
737 <https://doi.org/https://doi.org/10.1029/2005JD005810>
- 738 Li, J., Pósfai, M., Hobbs, P. v., & Buseck, P. R. (2003). Individual aerosol particles from biomass burning
739 in southern Africa: 2, Compositions and aging of inorganic particles. *Journal of Geophysical
740 Research: Atmospheres*, 108(D13). <https://doi.org/https://doi.org/10.1029/2002JD002310>
- 741 Maenhaut, W., Salma, I., Cafmeyer, J., Annegarn, H. J., & Andreae, M. O. (1996). Regional atmospheric
742 aerosol composition and sources in the eastern Transvaal, South Africa, and impact of biomass
743 burning. *Journal of Geophysical Research: Atmospheres*, 101(D19), 23631–23650.
744 <https://doi.org/https://doi.org/10.1029/95JD02930>
- 745 Massoli, P., Lambe, A. T., Ahern, A. T., Williams, L. R., Ehn, M., Mikkilä, J., Canagaratna, M. R.,
746 Brune, W. H., Onasch, T. B., Jayne, J. T., Petäjä, T., Kulmala, M., Laaksonen, A., Kolb, C. E.,
747 Davidovits, P., & Worsnop, D. R. (2010). Relationship between aerosol oxidation level and
748 hygroscopic properties of laboratory generated secondary organic aerosol (SOA) particles.
749 *Geophysical Research Letters*, 37(24). <https://doi.org/https://doi.org/10.1029/2010GL045258>
- 750 McCoy, D. T., Burrows, S. M., Wood, R., Grosvenor, D. P., Elliott, S. M., Ma, P.-L., Rasch, P. J., &
751 Hartment, D. L. (2022). Natural aerosols explain seasonal and spatial patterns of Southern Ocean
752 cloud albedo. *Science Advances*, 1(6), e1500157. <https://doi.org/10.1126/sciadv.1500157>
- 753 McFiggans, G., Artaxo, P., Baltensperger, U., Coe, H., Facchini, M. C., Feingold, G., Fuzzi, S., Gysel,
754 M., Laaksonen, A., Lohmann, U., Mentel, T. F., Murphy, D. M., O'Dowd, C. D., Snider, J. R., &
755 Weingartner, E. (2006). The effect of physical and chemical aerosol properties on warm cloud
756 droplet activation. *Atmospheric Chemistry and Physics*, 6(9), 2593–2649.
757 <https://doi.org/10.5194/acp-6-2593-2006>
- 758 Miles, J. C., Crutzen, P. J., & Goldammer, J. G. (1995). Fire in the Environment: The Ecological,
759 Atmospheric and Climatic Importance of Vegetation Fires. *Journal of Ecology*, 83, 549.
- 760 Miller, R. M., McFarquhar, G. M., Rauber, R. M., O'Brien, J. R., Gupta, S., Segal-Rozenhaimer, M.,
761 Dobracki, A. N., Sedlacek, A. J., Burton, S. P., Howell, S. G., Freitag, S., & Dang, C. (2021).
762 Observations of supermicron-sized aerosols originating from biomass burning in southern Central
763 Africa. *Atmos. Chem. Phys.*, 21(19), 14815–14831. <https://doi.org/10.5194/acp-21-14815-2021>
- 764 Moran-Zuloaga, D., Ditas, F., Walter, D., Saturno, J., Brito, J., Carbone, S., Chi, X., de Angelis, I., Baars,
765 H., Godoi, R. H. M., Heese, B., Holanda, B. A., Lavrič, J. v, Martin, S. T., Ming, J., Pöhlker, M. L.,
766 Ruckteschler, N., Su, H., Wang, Y., ... Pöhlker, C. (2018). Long-term study on coarse mode
767 aerosols in the Amazon rain forest with the frequent intrusion of Saharan dust plumes. *Atmospheric
768 Chemistry and Physics*, 18(13), 10055–10088. <https://doi.org/10.5194/acp-18-10055-2018>
- 769 Murphy, D. M., Cziczo, D. J., Froyd, K. D., Hudson, P. K., Matthew, B. M., Middlebrook, A. M., Peltier,
770 R. E., Sullivan, A., Thomson, D. S., & Weber, R. J. (2006). Single-particle mass spectrometry of
771 tropospheric aerosol particles. *Journal of Geophysical Research: Atmospheres*, 111(D23).
772 <https://doi.org/https://doi.org/10.1029/2006JD007340>



- 773 O’Dowd, C. D., & de Leeuw, G. (2007). Marine aerosol production: a review of the current knowledge.
774 *Philosophical Transactions of the Royal Society A: Mathematical, Physical and Engineering*
775 *Sciences*, 365(1856), 1753–1774. <https://doi.org/10.1098/rsta.2007.2043>
- 776 Ovadnevaite, J., Zuend, A., Laaksonen, A., Sanchez, K. J., Roberts, G., Ceburnis, D., Decesari, S.,
777 Rinaldi, M., Hodas, N., Facchini, M. C., Seinfeld, J. H., & O’ Dowd, C. (2017). Surface tension
778 prevails over solute effect in organic-influenced cloud droplet activation. *Nature*, 546(7660), 637–
779 641. <https://doi.org/10.1038/nature22806>
- 780 Petters, M. D., & Kreidenweis, S. M. (2007). A single parameter representation of hygroscopic growth
781 and cloud condensation nucleus activity. *Atmospheric Chemistry and Physics*, 7(8), 1961–1971.
782 <https://doi.org/10.5194/acp-7-1961-2007>
- 783 Pierce, J. R., Chen, K., & Adams, P. J. (2007). Contribution of primary carbonaceous aerosol to cloud
784 condensation nuclei: processes and uncertainties evaluated with a global aerosol microphysics
785 model. *Atmospheric Chemistry and Physics*, 7(20), 5447–5466. [https://doi.org/10.5194/acp-7-5447-](https://doi.org/10.5194/acp-7-5447-2007)
786 2007
- 787 Pöhlker, M. L., Pöhlker, C., Ditas, F., Klimach, T., de Angelis, I., Araújo, A., Brito, J., Carbone, S.,
788 Cheng, Y., Chi, X., Ditz, R., Gunthe, S. S., Kesselmeier, J., Könemann, T., Lavrič, J. v, Martin, S.
789 T., Mikhailov, E., Moran-Zuloaga, D., Rose, D., ... Pöschl, U. (2016). Long-term observations of
790 cloud condensation nuclei in the Amazon rain forest -- Part 1: Aerosol size distribution,
791 hygroscopicity, and new model parametrizations for CCN prediction. *Atmospheric Chemistry and*
792 *Physics*, 16(24), 15709–15740. <https://doi.org/10.5194/acp-16-15709-2016>
- 793 Pósfai, M., Simonics, R., Li, J., Hobbs, P. v, & Buseck, P. R. (2003). Individual aerosol particles from
794 biomass burning in southern Africa: 1. Compositions and size distributions of carbonaceous
795 particles. *Journal of Geophysical Research: Atmospheres*, 108(D13).
796 <https://doi.org/https://doi.org/10.1029/2002JD002291>
- 797 Prospero, J. M. (1968). atmospheric dust studies on Barbados. *Bulletin of the American Meteorological*
798 *Society*, 49(6), 645–652. <https://doi.org/10.1175/1520-0477-49.6.645>
- 799 Prospero, J. M. (1999). Long-range transport of mineral dust in the global atmosphere: Impact of African
800 dust on the environment of the southeastern United States. *Proceedings of the National Academy of*
801 *Sciences*, 96(7), 3396 LP – 3403. <https://doi.org/10.1073/pnas.96.7.3396>
- 802 Prospero, J. M., Barkley, A. E., Gaston, C. J., Gatineau, A., Campos y Sansano, A., & Panechou, K.
803 (2020). Characterizing and Quantifying African Dust Transport and Deposition to South America:
804 Implications for the Phosphorus Budget in the Amazon Basin. *Global Biogeochemical Cycles*,
805 34(9), e2020GB006536. <https://doi.org/https://doi.org/10.1029/2020GB006536>
- 806 Prospero, J. M., Blades, E., Mathison, G., & Naidu, R. (2005). Interhemispheric transport of viable fungi
807 and bacteria from Africa to the Caribbean with soil dust. *Aerobiologia*, 21(1), 1–19.
808 <https://doi.org/10.1007/s10453-004-5872-7>
- 809 Prospero, J. M., Collard, F.-X., Molinié, J., & Jeannot, A. (2014). Characterizing the annual cycle of
810 African dust transport to the Caribbean Basin and South America and its impact on the environment
811 and air quality. *Global Biogeochemical Cycles*, 28(7), 757–773.
812 <https://doi.org/https://doi.org/10.1002/2013GB004802>



- 813 Prospero, J. M., Delany, A. C., Delany, A. C., & Carlson, T. N. (2021). The Discovery of African Dust
814 Transport to the Western Hemisphere and the Saharan Air Layer: A History. *Bulletin of the*
815 *American Meteorological Society*, 102(6), E1239–E1260. <https://doi.org/10.1175/BAMS-D-19->
816 0309.1
- 817 Prospero, J. M., Glaccum, R. A., & Nees, R. T. (1981). Atmospheric transport of soil dust from Africa to
818 South America. *Nature*, 289(5798), 570–572. <https://doi.org/10.1038/289570a0>
- 819 Prospero, J. M., & Lamb, P. J. (n.d.). *prospero2003*.
- 820 Prospero, J. M., & Lamb, P. J. (2003). African Droughts and Dust Transport to the Caribbean: Climate
821 Change Implications. *Science*, 302(5647), 1024–1027. <https://doi.org/10.1126/science.1089915>
- 822 Prospero, J. M., & Mayol-Bracero, O. L. (2013). Understanding the Transport and Impact of African Dust
823 on the Caribbean Basin. *Bulletin of the American Meteorological Society*, 94(9), 1329–1337.
824 <https://doi.org/10.1175/BAMS-D-12-00142.1>
- 825 Quinn, P. K., Bates, T. S., Coffman, D. J., & Covert, D. S. (2008). Influence of particle size and
826 chemistry on the cloud nucleating properties of aerosols. *Atmospheric Chemistry and Physics*, 8(4),
827 1029–1042. <https://doi.org/10.5194/acp-8-1029-2008>
- 828 Quinn, P. K., Thompson, E. J., Coffman, D. J., Baidar, S., Bariteau, L., Bates, T. S., Bigorre, S., Brewer,
829 A., de Boer, G., de Szoeker, S. P., Drushka, K., Foltz, G. R., Intrieri, J., Iyer, S., Fairall, C. W.,
830 Gaston, C. J., Jansen, F., Johnson, J. E., Krüger, O. O., ... Zuidema, P. (2021). Measurements from
831 the RV Ronald H. Brown and related platforms as part of the Atlantic Tradewind Ocean-
832 Atmosphere Mesoscale Interaction Campaign (ATOMIC). *Earth Syst. Sci. Data*, 13(4), 1759–1790.
833 <https://doi.org/10.5194/essd-13-1759-2021>
- 834 Rauber, R. M., Stevens, B., Ochs, H. T., Knight, C., Albrecht, B. A., Blyth, A. M., Fairall, C. W., Jensen,
835 J. B., Lasher-Trapp, S. G., Mayol-Bracero, O. L., Vali, G., Anderson, J. R., Baker, B. A., Bandy, A.
836 R., Burnet, E., Brenguier, J.-L., Brewer, W. A., Brown, P. R. A., Chuang, R., ... Zuidema, P.
837 (2007). Rain in Shallow Cumulus Over the Ocean: The RICO Campaign. *Bulletin of the American*
838 *Meteorological Society*, 88(12), 1912–1928. <https://doi.org/10.1175/BAMS-88-12-1912>
- 839 Reid, J. S., Koppmann, R., Eck, T. F., & Eleuterio, D. P. (2005). A review of biomass burning emissions
840 part II: intensive physical properties of biomass burning particles. *Atmospheric Chemistry and*
841 *Physics*, 5(3), 799–825. <https://doi.org/10.5194/acp-5-799-2005>
- 842 Roberts, G. C., Artaxo, P., Zhou, J., Swietlicki, E., & Andreae, M. O. (2002). Sensitivity of CCN spectra
843 on chemical and physical properties of aerosol: A case study from the Amazon Basin. *Journal of*
844 *Geophysical Research: Atmospheres*, 107(D20), LBA 37-1-LBA 37-18.
845 <https://doi.org/10.1029/2001JD000583>
- 846 Roberts, G. C., & Nenes, A. (2005). A Continuous-Flow Streamwise Thermal-Gradient CCN Chamber
847 for Atmospheric Measurements. *Aerosol Science and Technology*, 39(3), 206–221.
848 <https://doi.org/10.1080/027868290913988>
- 849 Roberts, G., Wooster, M. J., & Lagoudakis, E. (2009). Annual and diurnal african biomass burning
850 temporal dynamics. *Biogeosciences*, 6(5), 849–866. <https://doi.org/10.5194/bg-6-849-2009>



- 851 Rolph, G., Stein, A., & Stunder, B. (2017). Real-time Environmental Applications and Display sYstem:
852 READY. *Environmental Modelling & Software*, 95, 210–228.
853 <https://doi.org/https://doi.org/10.1016/j.envsoft.2017.06.025>
- 854 Rose, D., Gunthe, S. S., Mikhailov, E., Frank, G. P., Dusek, U., Andreae, M. O., & Pöschl, U. (2008).
855 Calibration and measurement uncertainties of a continuous-flow cloud condensation nuclei counter
856 (DMT-CCNC): CCN activation of ammonium sulfate and sodium chloride aerosol particles in
857 theory and experiment. *Atmospheric Chemistry and Physics*, 8(5), 1153–1179.
858 <https://doi.org/10.5194/acp-8-1153-2008>
- 859 Rosenfeld, D., Rudich, Y., & Lahav, R. (2001). Desert dust suppressing precipitation: A possible
860 desertification feedback loop. *Proceedings of the National Academy of Sciences*, 98(11), 5975 LP –
861 5980. <https://doi.org/10.1073/pnas.101122798>
- 862 Russell, L. M., Hawkins, L. N., Frossard, A. A., Quinn, P. K., & Bates, T. S. (2010). Carbohydrate-like
863 composition of submicron atmospheric particles and their production from ocean bubble bursting.
864 *Proceedings of the National Academy of Sciences*, 107(15), 6652 LP – 6657.
865 <https://doi.org/10.1073/pnas.0908905107>
- 866 Savoie, D. L., Arimoto, R., Keene, W. C., Prospero, J. M., Duce, R. A., & Galloway, J. N. (2002). Marine
867 biogenic and anthropogenic contributions to non-sea-salt sulfate in the marine boundary layer over
868 the North Atlantic Ocean. *Journal of Geophysical Research: Atmospheres*, 107(D18), AAC 3-1-
869 AAC 3-21. <https://doi.org/https://doi.org/10.1029/2001JD000970>
- 870 Schill, G. P., Froyd, K. D., Bian, H., Kupc, A., Williamson, C., Brock, C. A., Ray, E., Hornbrook, R. S.,
871 Hills, A. J., Apel, E. C., Chin, M., Colarco, P. R., & Murphy, D. M. (2020). Widespread biomass
872 burning smoke throughout the remote troposphere. *Nature Geoscience*, 13(6), 422–427.
873 <https://doi.org/10.1038/s41561-020-0586-1>
- 874 Shen, H., Peters, T. M., Casuccio, G. S., Lersch, T. L., West, R. R., Kumar, A., Kumar, N., & Ault, A. P.
875 (2016). Elevated Concentrations of Lead in Particulate Matter on the Neighborhood-Scale in Delhi,
876 India As Determined by Single Particle Analysis. *Environmental Science & Technology*, 50(10),
877 4961–4970. <https://doi.org/10.1021/acs.est.5b06202>
- 878 Sobanska, S., Coeur, C., Maenhaut, W., & Adams, F. (2003). SEM-EDX Characterisation of
879 Tropospheric Aerosols in the Negev Desert (Israel). *Journal of Atmospheric Chemistry*, 44(3), 299–
880 322. <https://doi.org/10.1023/A:1022969302107>
- 881 Sorooshian, A., Corral, A. F., Braun, R. A., Cairns, B., Crosbie, E., Ferrare, R., Hair, J., Kleb, M. M.,
882 Hossein Mardi, A., Maring, H., McComiskey, A., Moore, R., Painemal, D., Scarino, A. J.,
883 Schlosser, J., Shingler, T., Shook, M., Wang, H., Zeng, X., ... Zuidema, P. (2020). Atmospheric
884 Research Over the Western North Atlantic Ocean Region and North American East Coast: A
885 Review of Past Work and Challenges Ahead. *Journal of Geophysical Research: Atmospheres*,
886 125(6), e2019JD031626. <https://doi.org/https://doi.org/10.1029/2019JD031626>
- 887 Spracklen, D. v, Carslaw, K. S., Pöschl, U., Rap, A., & Forster, P. M. (2011). Global cloud condensation
888 nuclei influenced by carbonaceous combustion aerosol. *Atmospheric Chemistry and Physics*, 11(17),
889 9067–9087. <https://doi.org/10.5194/acp-11-9067-2011>



- 890 Stein, A. F., Draxler, R. R., Rolph, G. D., Stunder, B. J. B., Cohen, M. D., & Ngan, F. (2015). NOAA's
891 HYSPLIT Atmospheric Transport and Dispersion Modeling System. *Bulletin of the American*
892 *Meteorological Society*, 96(12), 2059–2077. <https://doi.org/10.1175/BAMS-D-14-00110.1>
- 893 Stevens, B., Bony, S., Farrell, D., Ament, F., Blyth, A., Fairall, C., Karstensen, J., Quinn, P. K., Speich,
894 S., Acquistapace, C., Aemisegger, F., Albright, A. L., Bellenger, H., Bodenschatz, E., Caesar, K.-A.,
895 Chewitt-Lucas, R., de Boer, G., Delanoë, J., Denby, L., ... Zöger, M. (2021). EUREC4A. *Earth*
896 *Syst. Sci. Data*, 13(8), 4067–4119. <https://doi.org/10.5194/essd-13-4067-2021>
- 897 Stevens, B., Farrell, D., Hirsch, L., Jansen, F., Nuijens, L., Serikov, I., Brüggemann, B., Forde, M., Linne,
898 H., Lonitz, K., & Prospero, J. M. (2016). The Barbados Cloud Observatory: Anchoring
899 Investigations of Clouds and Circulation on the Edge of the ITCZ. *Bulletin of the American*
900 *Meteorological Society*, 97(5), 787–801. <https://doi.org/10.1175/BAMS-D-14-00247.1>
- 901 Tomlin, J. M., Jankowski, K. A., Veghte, D. P., China, S., Wang, P., Fraund, M., Weis, J., Zheng, G.,
902 Wang, Y., Rivera-Adorno, F., Raveh-Rubin, S., Knopf, D. A., Wang, J., Gilles, M. K., Moffet, R.
903 C., & Laskin, A. (2021). Impact of dry intrusion events on the composition and mixing state of
904 particles during the winter Aerosol and Cloud Experiment in the Eastern North Atlantic (ACE-
905 ENA). *Atmospheric Chemistry and Physics*, 21(24), 18123–18146. [https://doi.org/10.5194/acp-21-](https://doi.org/10.5194/acp-21-18123-2021)
906 [18123-2021](https://doi.org/10.5194/acp-21-18123-2021)
- 907 Twohy, C. H., Kreidenweis, S. M., Eidhammer, T., Browell, E. v., Heymsfield, A. J., Bansemer, A. R.,
908 Anderson, B. E., Chen, G., Ismail, S., DeMott, P. J., & van den Heever, S. C. (2009). Saharan dust
909 particles nucleate droplets in eastern Atlantic clouds. *Geophysical Research Letters*.
910 <https://doi.org/10.1029/2008GL035846>
- 911 Twomey, S. (1974). Pollution and the planetary albedo. *Atmospheric Environment (1967)*, 8(12), 1251–
912 1256. [https://doi.org/https://doi.org/10.1016/0004-6981\(74\)90004-3](https://doi.org/https://doi.org/10.1016/0004-6981(74)90004-3)
- 913 Twomey, S. (1977). The Influence of Pollution on the Shortwave Albedo of Clouds. *Journal of*
914 *Atmospheric Sciences*, 34(7), 1149–1152. [https://doi.org/10.1175/1520-](https://doi.org/10.1175/1520-0469(1977)034<1149:TIOPOT>2.0.CO;2)
915 [0469\(1977\)034<1149:TIOPOT>2.0.CO;2](https://doi.org/10.1175/1520-0469(1977)034<1149:TIOPOT>2.0.CO;2)
- 916 Wex, H., Dieckmann, K., Roberts, G. C., Conrath, T., Izaguirre, M. A., Hartmann, S., Herenz, P., Schäfer,
917 M., Ditas, F., Schmeissner, T., Henning, S., Wehner, B., Siebert, H., & Stratmann, F. (2016).
918 Aerosol arriving on the Caribbean island of Barbados: physical properties and origin. *Atmos. Chem.*
919 *Phys.*, 16(22), 14107–14130. <https://doi.org/10.5194/acp-16-14107-2016>
- 920 Yu, H., Tan, Q., Chin, M., Remer, L. A., Kahn, R. A., Bian, H., Kim, D., Zhang, Z., Yuan, T., Omar, A.
921 H., Winker, D. M., Levy, R., Kalashnikova, O., Crepeau, L., Capelle, V., & Chedin, A. (2019).
922 Estimates of African Dust Deposition Along the Trans-Atlantic Transit Using the Decade-long
923 Record of Aerosol Measurements from CALIOP, MODIS, MISR, and IASI. *Journal of Geophysical*
924 *Research. Atmospheres : JGR*, 124(14), 7975–7996. <https://doi.org/10.1029/2019JD030574>
- 925 Zauscher, M. D., Wang, Y., Moore, M. J. K., Gaston, C. J., & Prather, K. A. (2013). Air Quality Impact
926 and Physicochemical Aging of Biomass Burning Aerosols during the 2007 San Diego Wildfires.
927 *Environmental Science & Technology*, 47(14), 7633–7643. <https://doi.org/10.1021/es4004137>
- 928 Zuidema, P., Alvarez, C., Kramer, S. J., Custals, L., Izaguirre, M., Sealy, P., Prospero, J. M., & Blades, E.
929 (2019). Is Summer African Dust Arriving Earlier to Barbados? The Updated Long-Term In Situ
930 Dust Mass Concentration Time Series from Ragged Point, Barbados, and Miami, Florida. *Bulletin of*



- 931 *the American Meteorological Society*, 100(10), 1981–1986. [https://doi.org/10.1175/BAMS-D-18-](https://doi.org/10.1175/BAMS-D-18-0083.1)
932 0083.1
- 933 Zuidema, P., Sedlacek III, A. J., Flynn, C., Springston, S., Delgadillo, R., Zhang, J., Aiken, A. C.,
934 Koontz, A., & Muradyan, P. (2018). The Ascension Island Boundary Layer in the Remote Southeast
935 Atlantic is Often Smoky. *Geophysical Research Letters*, 45(9), 4456–4465.
936 <https://doi.org/https://doi.org/10.1002/2017GL076926>
- 937 Zuidema, P., Xue, H., & Feingold, G. (2008). Shortwave Radiative Impacts from Aerosol Effects on
938 Marine Shallow Cumuli. *Journal of the Atmospheric Sciences*, 65(6), 1979–1990.
939 <https://doi.org/10.1175/2007JAS2447.1>
- 940
- 941